Supporting Information for

Facile separation of cyclic aliphatic and aromatic vapors using crystalline thiacalixarene assemblies with preorganized channels

Manabu Yamada,*[a] Ruka Yoshizaki,[a] Fumiya Uemura,[a] Hiroshi Katagiri,*[b] Sumio Kato,[a] Kazuhiko Akimoto[c] and Fumio Hamada[d]

[a] Department of Materials Science, Graduate School of Engineering Science, Akita University, 1-1 Tegatagakuen-machi, Akita 010-8502, Japan
[b] Graduate School of Organic Materials Science, Yamagata University, 4-3-16, Jonan, Yonezawa, Yamagata 992-8510, Japan
[c] Nissan Chemical Industries, LTD, 6903-1 Ooaza-Onoda, Sanyo-Onoda, Yamaguchi 756-0093, Japan
[d] Emeritus Professor, Akita University, 1-1 Tegatagakuen-machi, Akita 010-8502, Japan

*Corresponding authors.
Tel +81 18 889 3068; fax: +81 18 889 3068
E-mail address: myamada@gipc.akita-u.ac.jp (M.Y.)

Tel +81 238 26 3743; fax: +81 238 26 3743
E-mail address: kgri7078@yz.yamagata-u.ac.jp (H.K.)

Table of Contents

Fig. S5 ^{1}H NMR spectra of **1α** incorporating CyC_6 and Bz after a) 0 h, b) 1 h, c) 2 h, d) 3 h, e) 6 h of air aging.

Fig. S6 ^{1}H NMR spectra of **1α** incorporating $MeCyC_6$ and Tol after a) 0 h, b) 1 h, c) 2 h, d) 3 h, e) 6 h of air aging.

Fig. S7 Preliminary data of head-space gas chromatograms of the remaining ratio of CyC_6 and Bz in **1α** after a) 0 h, b) 1 h, c) 2 h, d) 3 h, and e) 6 h of air aging.

Fig. S8 Preliminary data of head-space gas chromatograms of the remaining ratio of $MeCyC_6$ and Tol in **1α** after a) 0 h, b) 1 h, c) 2 h, d) 3 h, and e) 6 h of air aging.

Fig. S9 ORTEP diagram of **1**·$MeCyC_6$ with thermal ellipsoids at 50 % probability. Color code: bromine (purple), sulfur (yellow), oxygen (red), carbon (black), and hydrogen (light green).

Fig. S10 ORTEP diagram of **1**·Bz with thermal ellipsoids at 50 % probability. Color code: bromine (purple), sulfur (yellow), oxygen (red), carbon (black), and hydrogen (light green).

Fig. S11 ORTEP diagram of **1**·Tol with thermal ellipsoids at 50 % probability. Color code: bromine (purple), sulfur (yellow), oxygen (red), carbon (black), and hydrogen (light green).

Fig. S12 Extended crystal structures of a) **1**·$MeCyC_6$, b) **1**·Bz, and c) **1**·Tol. Color code: bromine (brown), sulfur (yellow), oxygen (red), carbon (dark gray), and hydrogen (light gray). Bz molecules are shown as space-filling models.

Fig. S13 ^{1}H NMR spectrum of the crystal **1**·Bz dissolved in chloroform-d_1 ($CDCl_3$, δ from TMS).

Fig. S14 ^{1}H NMR spectrum of the crystal a) **1**·$MeCyC_6$ and b) **1**·Tol dissolved in chloroform-d_1 (500 MHz, $CDCl_3$, δ from TMS).

Fig. S15 Le Bail fit for the **1α**-adsorbed $MeCyC_6$ against the experimental powder X-ray diffraction (PXRD) pattern. The red crosses represent the experimental pattern, and the pale blue line represents the refined fit. The background (black), difference plot (blue), and Bragg position (green) are also displayed.

Fig. S16 Le Bail fit for the **1α**-adsorbed Bz against the experimental powder X-ray diffraction (PXRD) pattern. The red crosses represent the experimental pattern, and the pale blue line represents the refined fit. The background (black), difference plot (blue), and Bragg position (green) are also displayed.

Fig. S17 Le Bail fit for the **1α**-adsorbed Tol against the experimental powder X-ray diffraction pattern (PXRD) pattern. The red crosses represent displaying the experimental pattern, and the pale blue line represents the refined fit. The background (black), difference plot (blue), and Bragg position (green) are also displayed.

Fig. S18 Le Bail fit for the **1α**-adsorbed CyC_6/Bz against the experimental powder X-ray diffraction (PXRD) pattern. The red crosses represent the experimental pattern, and the pale blue line represents the refined fit. The background (black), difference plot (blue), and Bragg position (green) are also displayed.

Fig. S19 Le Bail fit for the **1α**-adsorbed $MeCyC_6$/Tol against the experimental powder X-ray diffraction (PXRD) pattern. The red crosses represent the experimental pattern, and the pale blue line represents the refined fit. The background (black), difference plot (blue), and Bragg position (green) are also displayed.

3. References

1. Experimental Section

Materials

All solvents were purchased from commercial sources and used as received. The reactions were carried out in a nitrogen atmosphere. *p*-Bromothiacalix[4]arene propyl ether molecules as a 1,3-alternate conformer were also synthesized according to the literature.[S1, S2]

Methods

Solution ^{1}H NMR

Solution ^{1}H NMR spectra were recorded at 500 MHz JEOL ECA500 instrument. Chemical shifts are quoted as parts per million (ppm) relative to tetramethylsilane ($CDCl_3$).

Powder X-ray diffraction

Powder X-ray diffraction (PXRD) patterns were collected with a Rigaku Ultima IV diffractometer with Cu Kα radiation (λ = 1.5406 Å, 40 kV, 40 mA) and a graphite monochromator at a step width of 0.02º 2θ and a scan speed of 2.000º min^{-1}.

Growth of methylcyclohexane included single crystals of 1·methylcyclohexane (**1**·$MeCyC_6$)

200 mg of activated **1α** was dissolved in methylcyclohexane/$CHCl_3$ mixed solution in a vial. The resulting solutions were allowed to slowly evaporate at room temperature over several days to afford colorless large crystals. The resultant crystals were conducted for analysis of single-crystal diffraction, PXRD, and NMR studies.

Growth of benzene included single crystals of 1· benzene (**1**·Bz)

200 mg of activated **1α** was dissolved in benzene (Bz) in a vial. The resulting solutions were allowed to slowly evaporate at room temperature over several days to afford colorless large crystals. The resultant crystals were conducted for analysis of single-crystal diffraction, PXRD, and NMR studies.

Growth of toluene included single crystals of 1· toluene (1·Tol**)**

200 mg of activated **1α** was dissolved in 2 mL of toluene in a vial. The resulting solutions were allowed to slowly evaporate at room temperature over several days to afford colorless large crystals. The resultant crystals were conducted for analysis of single-crystal diffraction, PXRD, and NMR studies.

X-ray crystallography of 1·Bz

Single crystals of **1**·Bz suitable for single-crystal X-ray diffraction studies were formed. The crystals in the mother liquid were picked up with a pipette and dropped in paraton oil. The single crystals coated with oil were isolated on MicroMounts, and the crystals were immediately placed in a cold nitrogen stream. X-Ray diffraction data for **1**·Bz were collected on a Rigaku XtaLAB Synergy-DW with multi-layer mirror optics Cu Kα radiation. The structures were solved by direct methods using SHELXT (Version 2015)[S3] and refined using the full-matrix least-squares method on F^2 using the SHELXL (Version 2018)[S4] Program. All materials for publication were prepared by Olex 2 1.3 software[S5]. All non-hydrogen atoms were refined anisotropically. The H atoms attached to O atoms were located by differential Fourier analysis and refined with U_{iso}(H) values of 1.5U_{eq}(O). The positions of other H atoms were calculated geometrically and refined as riding, with U_{iso} (H) values of 1.2U_{eq}(C).

X-ray crystallography of 1·MeCyC$_6$ and 1·Tol

Single crystals of **1**·MeCyC$_6$ and **1**·Tol suitable for single-crystal X-ray diffraction studies were formed. The crystals in the mother liquid were picked up with a pipette and dropped in paraton oil. The single crystals coated with oil were isolated on MicroMounts, and the crystals were immediately placed in a cold nitrogen stream. X-Ray diffraction data for **1**·MeCyC$_6$, **1**·Bz, and **1**·Tol were collected on a Rigaku XtaLAB P200 with graphite-monochromated Mo Kα radiation. The structures were solved by direct methods using SHELXT (Version 2014)[S3] and refined using the full-matrix least-squares method on F^2 using the SHELXL (Version 2014)[S4] Program. All materials for publication were prepared by Yadokari XG software[S6,S7]. All non-hydrogen atoms were refined anisotropically. The H atoms attached to O atoms were located by differential Fourier analysis and refined with U_{iso}(H) values of 1.5U_{eq}(O). The positions of other H atoms were calculated geometrically and refined as riding, with U_{iso} (H) values of 1.2U_{eq}(C).

Refinement details of the crystal 1·Bz: one propyl group of the **1** molecule and two Bz molecules were determined as disordered species. similarly, the number of Bz molecules was determined by the ^{1}H NMR spectrum (Fig. S13).

Refinement details of the crystal 1·MeCyC$_6$: two propyl groups of the **1** molecule were determined to be disordered species. In addition, the crystal **1**·MeCyC$_6$ retains the solvent electron density in the voids of the 3540 Å^3 / unit cell. The contribution of solvent electron density, 684 electrons, was removed by the SQUEEZE function[S8]. On the other hand, the solvent electron density in the voids was determined as MeCyC$_6$ molecules by the ^{1}H NMR spectrum (Fig. S14).

Refinement details of the crystal 1·Tol: two propyl groups of the **1** molecule were determined as disordered species. In addition, the crystal **1**·Tol retained the solvent

electron density in the voids of the 3418 Å^3/unit cell. The contribution of solvent electron density, 796 electrons, was removed by the SQUEEZE function[S8]. On the other hand, the solvent electron density in the voids was determined as Tol molecules by the ^{1}H NMR spectrum (Fig. S14).

Crystallographic Data

Table S1. Experimental single-crystal X-ray data for **1**·$MeCyC_6$, **1**·Bz, and **1**·Tol.

	1·$MeCyC_6$	**1**·Bz	**1**·Tol
Crystallization Solvent	$MeCyC_6/CHCl_3$ (=1:1)	benzene	toluene
Collection Temperature (K)	223	223	223
Formula	$C_{40.41}H_{44.82}Br_4O_4S_4$	$C_{42}H_{42}Br_4O_4S_4$	$C_{43}H_{44}Br_4O_4S_4$
Formula Weight	1045.38	1058.63	1072.66
Crystal System	trigonal	trigonal	trigonal
Space Group	$R\bar{3}c$	$R\bar{3}c$	$R\bar{3}c$
a [Å]	31.1921(6)	31.1234(3)	31.2941(5)
b [Å]	31.1921(6)	31.1234(3)	31.2941(5)
c [Å]	24.1196(5)	24.1605(2)	24.1681(4)
α [º]	90	90	90
β [º]	90	90	90
γ [º]	120	120	120
V [Å^3]	20323.1(9)	20268.0(4)	20497.4(7)
Z	18	18	18
D_{calcd} [g cm^{-1}]	1.533	1.561	1.564
F(000)	9419	9540	9684
θ_{max} [º]	26.1960	76.7030	28.6690
Reflections collected / unique	84595/28801 [R_{int} = 0.0637]	22078 / 11899 [R_{int} = 0.0439]	92214 / 26301 [R_{int} = 0.0473]
Data / restraints / parameter	28801 / 38/ 249	11899 / 245 / 337	26301 / 72 / 274
Final R indices [$I>2\sigma$ (I)]	$R1$ = 0.0423	$R1$ = 0.0563	$R1$ = 0.0449
	$wR2$ = 0.0894	$wR2$ = 0.1540	$wR2$ = 0.1041
R indices (all data)	$R1$ = 0.0646	$R1$ = 0.0612	$R1$ = 0.0693
	$wR2$ = 0.0984	$wR2$ = 0.1584	$wR2$ = 0.1177
Good-of-fit on F^2	1.026	1.032	1.029
Largest different peak and hole [e.A^{-3}]	0.630 and -0.418	1.043 and -0.550	0.733 and -0.430
CCDC	2212208	2212209	2212210

Vapor sorption measurement of the activated crystal 1α toward cyclohexane, methylcyclohexane, benzene, and toluene

Pre-treatment: Before vapor adsorption measurement, the activated crystal **1α** has been pretreated at 100°C at < 10^{-3} Torr for 1 day for **1** just before use by the installed equipment of a BELSORP 18 automated gas adsorption apparatus. The two cyclic aliphatics, cyclohexane and methylcyclohexane, were treated with CaH_2 to remove water as an impurity component, followed by distillation at N_2 atmosphere, and were stored by using molecular sieves 3A. The two aromatics, benzene and toluene, were treated with Na to remove water as an impurity component, followed by distillation in N_2 atmosphere, and were stored by using molecular sieves 3A.

Vapor adsorption measurement: Adsorption measurement of **1α** for the two aliphatic and two aromatic vapors was conducted by using the BELSORP 18 automated gas adsorption apparatus. The activated crystal **1α** was placed in the sample chamber (ca. 15 mL) and maintained at 25.0 ± 0.1°C. The larger gas chamber (176.36 mL) with a pressure gauge was kept at 50 ± 0.1°C. Helium gas at certain pressure was introduced into the gas chamber and was allowed to diffuse into the sample chamber by opening a valve. The change in pressure allowed an accurate determination of the volume of the total gas phase. Host-guest complexation was monitored similarly by using a guest vapor in place of helium. The amount of guest adsorbed was calculated readily from the pressure difference ($P_{cal} - P$), where, P_{cal} is the calculated pressure if there were no guest adsorption, as in the case of helium, and P is the observed equilibrium pressure, as which the change in pressure in 500 s had become smaller than 1 % of the pressure at the point. All operations were computer-controlled and automatic.

Thermogravimetric analysis (TGA)

Thermogravimetric analysis (TGA) was performed on a HITACHI STA7300 apparatus in the temperature range between 24 and 500 ºC under a N_2 atmosphere at a heating rate of 10 ºC min^{-1}.

Gas chromatography with the head-space method

Gas chromatography (GC) analysis was performed on a Shimazu GC-2010 Plus instrument with a DB-624 column (0.53 mm ID × 30 m, 0.3 μm) using the head-space method (a PerkinElmer TurboMatrix HS 40). The oven was set at 40 °C and ramped up at 10 °C min^{-1} increments to 240 °C and maintained for 10 min. The total run time was 60 min. The injection temperature was 140 °C, and the detection temperature was 250 °C. The flow rate (line velocity) was 35 cm sec^{-1} with helium as the carrier gas.

Refinement of powder X-ray diffraction (PXRD) patterns for the 1α-adsorbed $MeCyC_6$, Bz, Tol, CyC_6/Bz, and $MeCyC_6$/Tol vapors using Le Bail fit

The PXRD patterns of the **1α**-adsorbed $MeCyC_6$, Bz, Tol, CyC_6/Bz, and $MeCyC_6$/Tol vapors were refined using the Le Bail method[S9] using RIETAN-FP software[S10]. The simulated PXRD patterns of the single-crystal X-ray structures of **1**·$MeCyC_6$, **1**·Bz, and **1**·Tol matched the measured PXRD patterns. Therefore, the lattice constants obtained from the single crystal X-ray structure analyses of **1**·$MeCyC_6$, **1**·Bz, and **1**·Tol were employed in the Le Bail fit. For the refinement of PXRD patterns after **1α** adsorbed $MeCyC_6$, Bz, and Tol, the lattice constants of the corresponding single crystals were used as initial values. In contrast, for the refinement of PXRD patterns after **1α** adsorbed CyC_6/Bz or $MeCyC_6$/Tol, the lattice constants of single-crystal X-ray structures of **1**·Bz or **1**·Tol were used as initial values. In this fit, the refinement of each PXRD pattern was performed by pattern-fitting the lattice constant or the zero-point shift while keeping one

value fixed and varying the other. The final unit cell parameters, along with the residual values of R_p and R_{wp}, were refined (Fig. S15 – S19).

2. Supporting figures

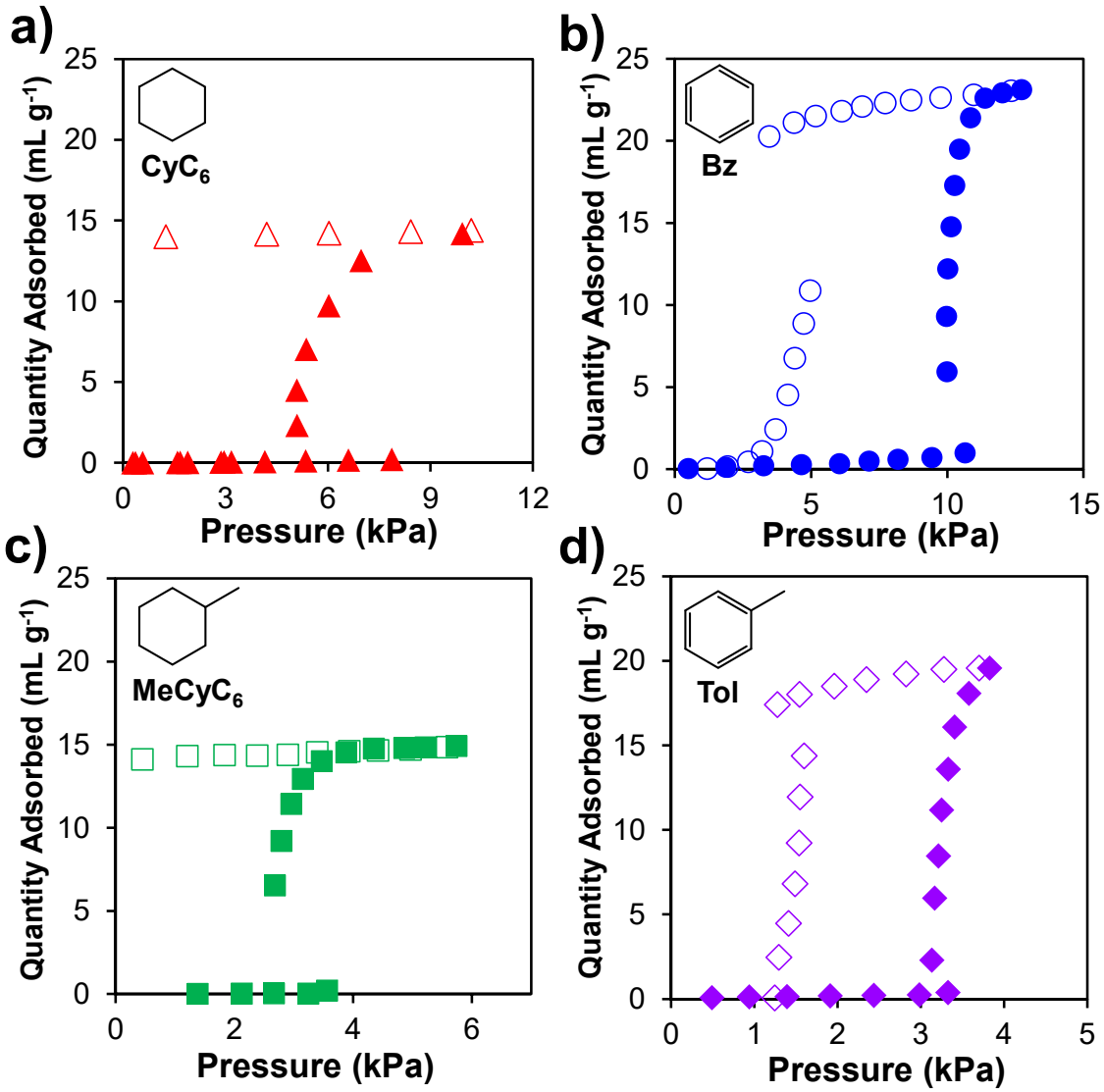

Fig. S1 Vapor sorption isotherms of **1α** at 25 °C in a) CyC_6, b) Bz, c) $MeCyC_6$, and d) Tol vapor. Solid symbols: sorption; open symbols: desorption.

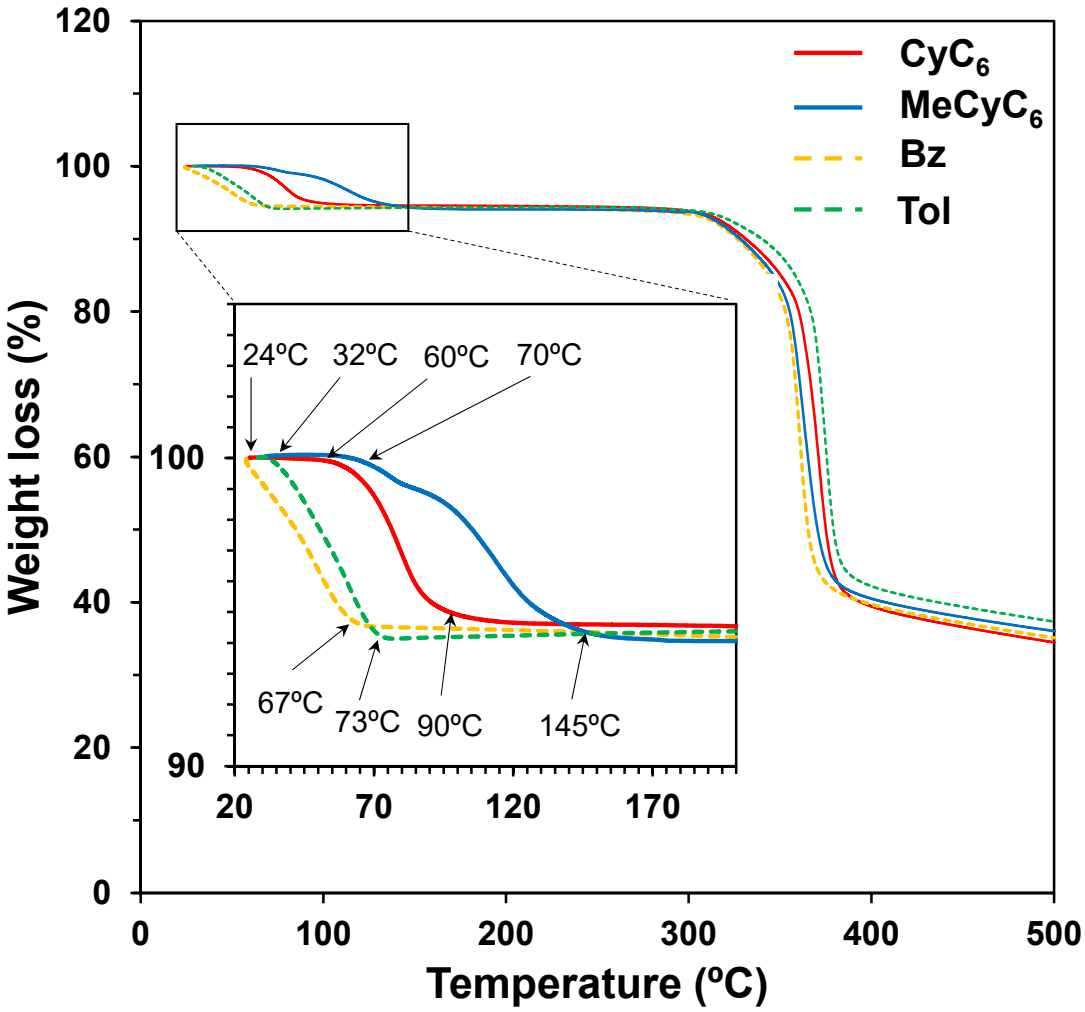

Fig. S2 Thermogravimetric analysis (TGA) of the **1α**-adsorbed CyC_6 (red line), $MeCyC_6$ (blue line), Bz (yellow dotted line), and Tol (green dotted line).

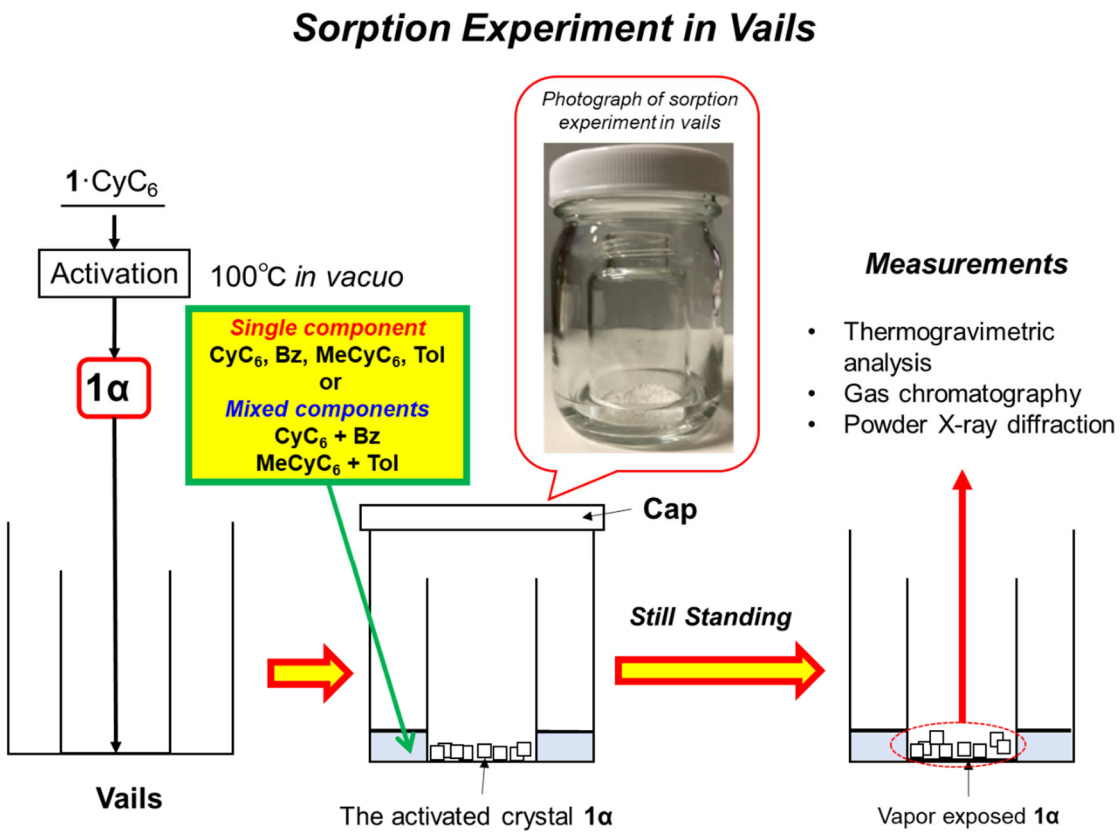

Fig. S3 Vapor sorption experiments of activated crystal **1α** for single or two components of cyclic aliphatics and aromatics in vials.

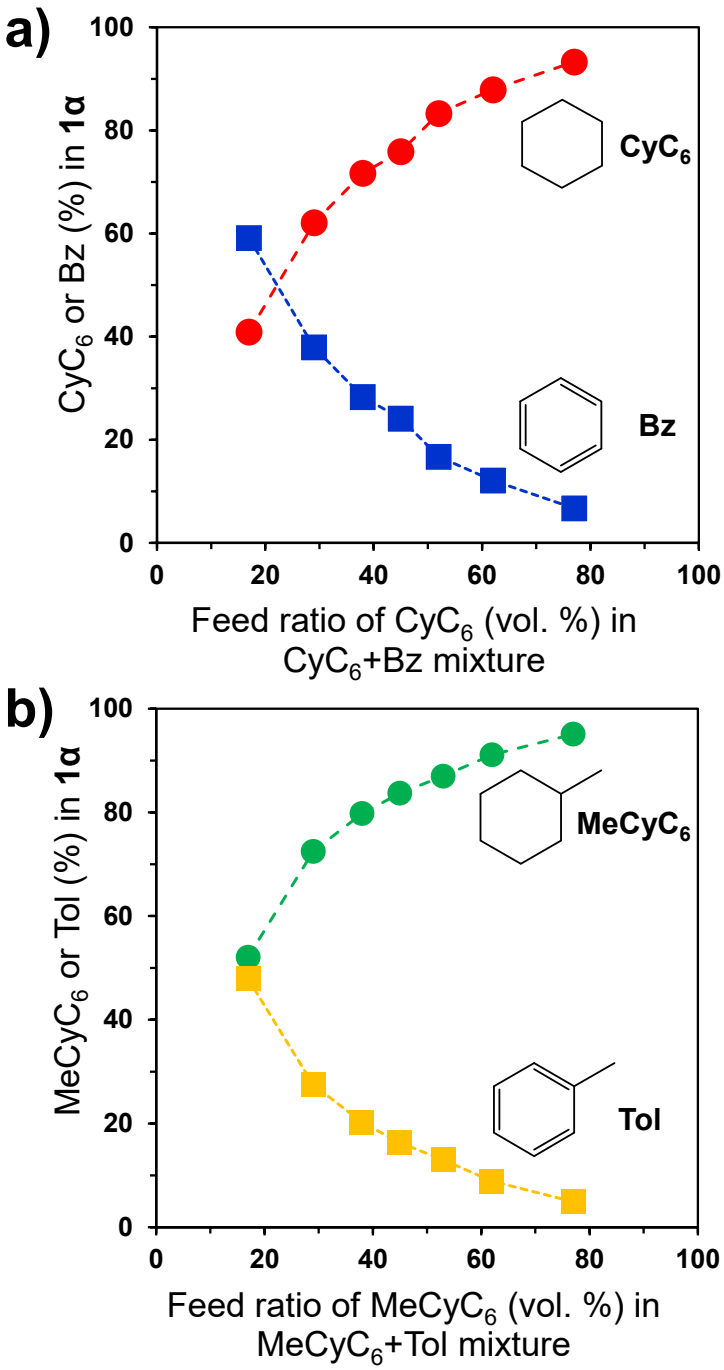

Fig. S4 Head-space gas chromatography of the adsorption ratio (%) of a) CyC_6/Bz or b) $MeCyC_6$/Tol in **1α** exposed to a CyC_6/Bz or $MeCyC_6$/Tol mixed system at various compositions 1:4–1:0.25 (v/v) for 48 h

The results of head-space GC measurements indicated that the adsorbed amounts of CyC_6 and $MeCyC_6$ in **1α** range from 40.9 % to 93.3 % and from 52.1 % to 95.1 %, respectively. In contrast, the adsorbed quantities of aromatic hydrocarbons decreased, and the amounts of the adsorbed Bz and Tol ranged from 59.1 % to 6.7 % and from 47.9 % to 4.9 %, respectively.

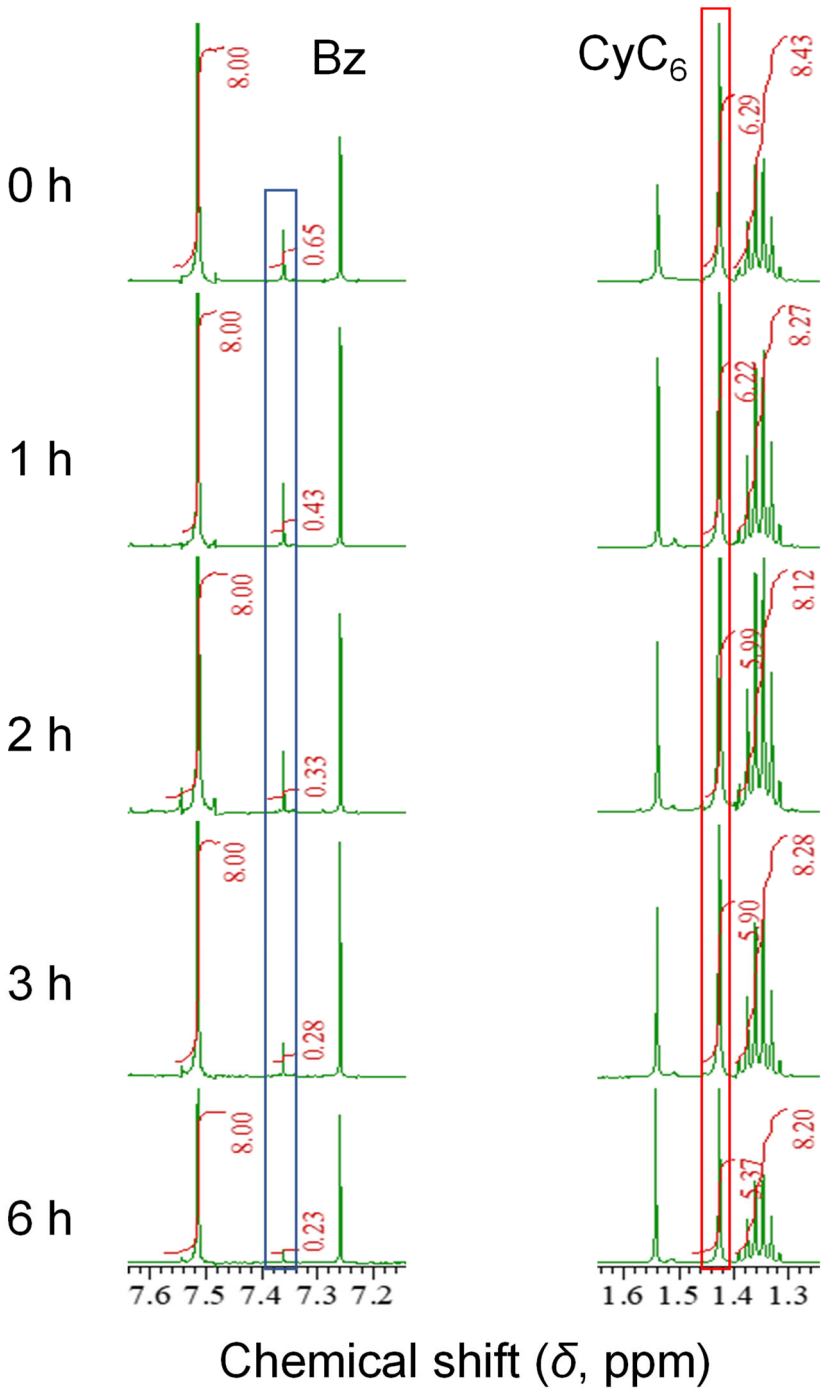

Fig. S5 ^{1}H NMR spectra of **1α** incorporating CyC_6 and Bz after a) 0 h, b) 1 h, c) 2 h, d) 3 h, and e) 6 h of air aging.

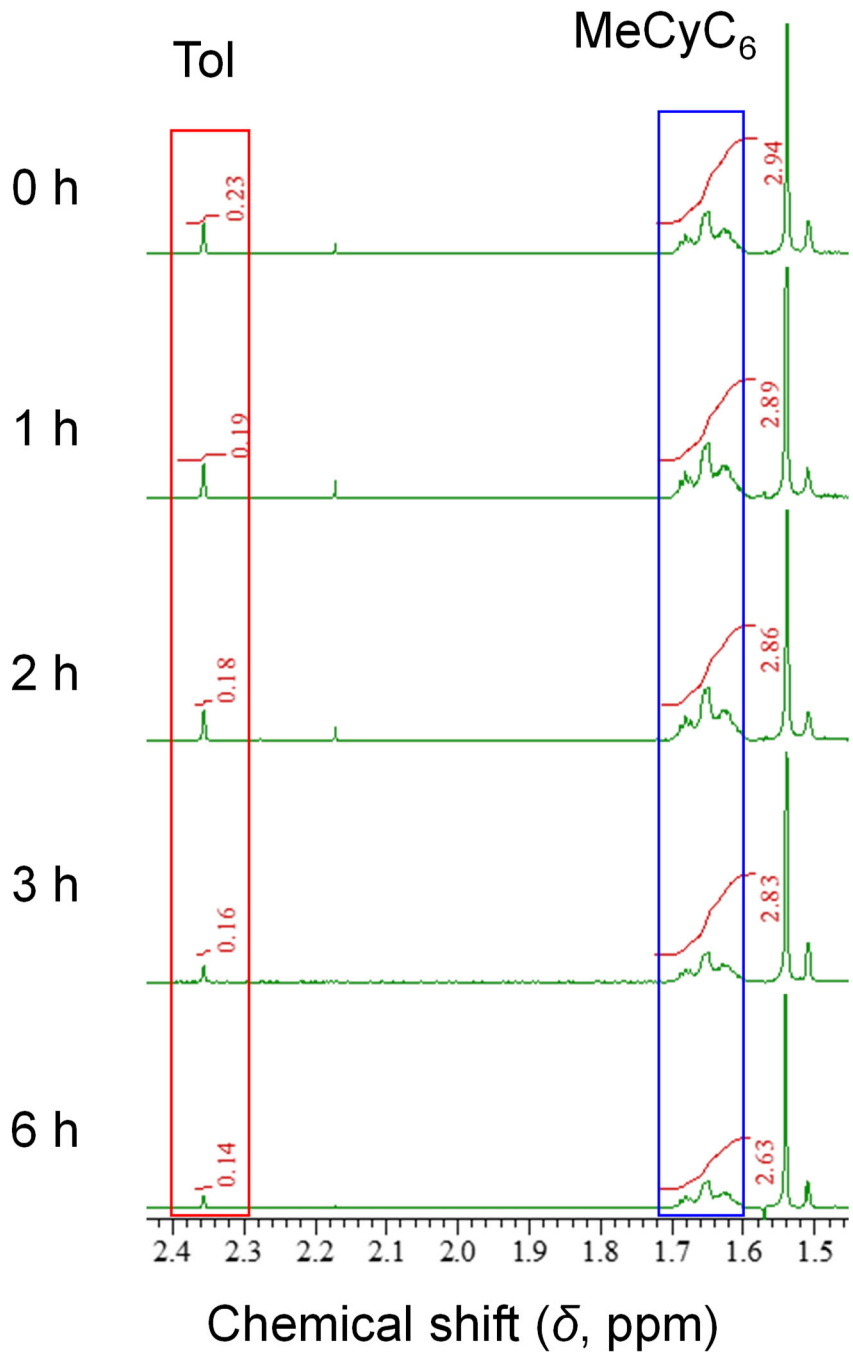

Fig. S6 ^{1}H NMR spectra of **1α** incorporating $MeCyC_6$ and Tol after a) 0 h, b) 1 h, c) 2 h, d) 3 h, and e) 6 h of air aging.

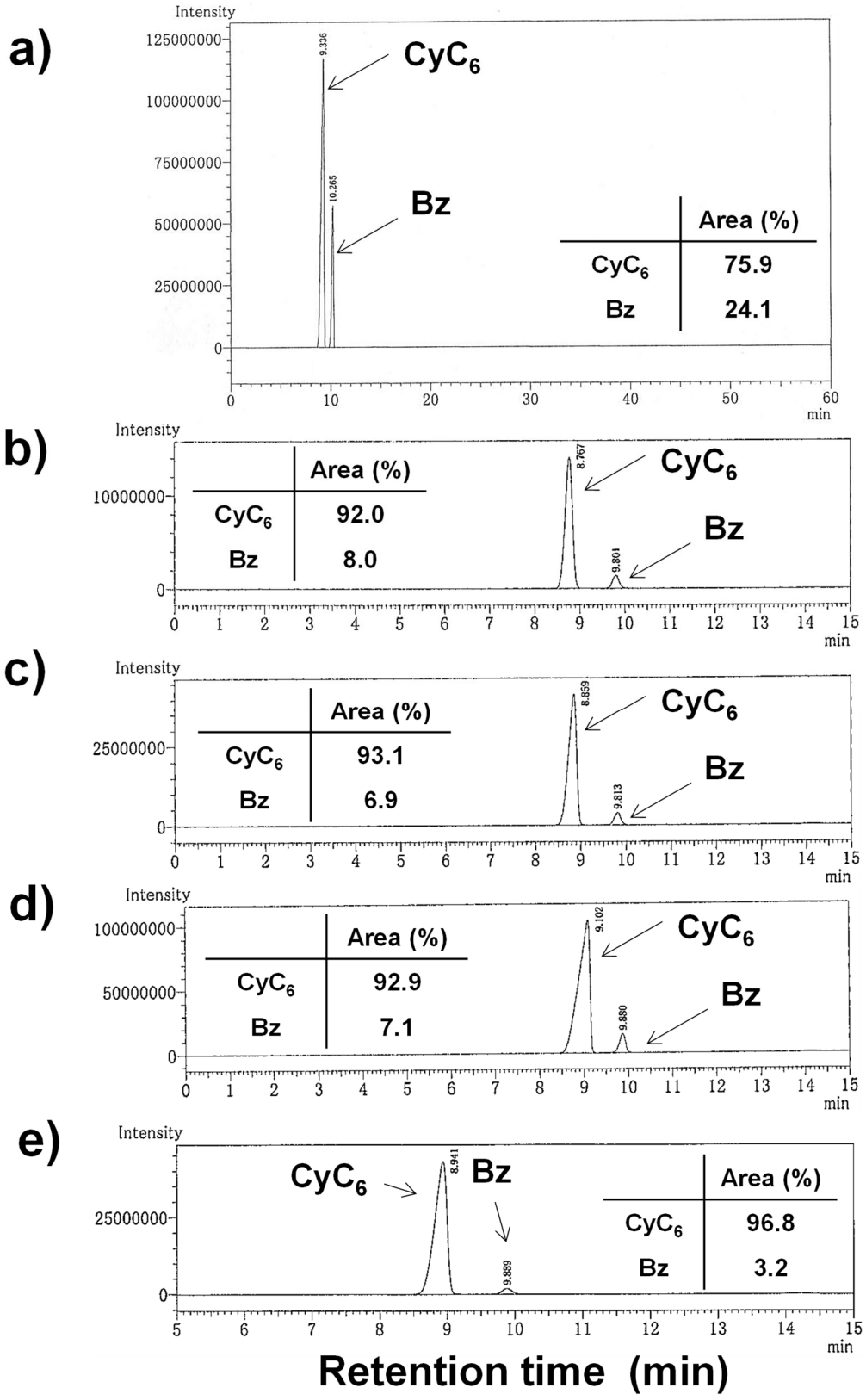

Fig. S7 Preliminary data of head-space gas chromatograms of the remaining ratio of CyC_6 and Bz in **1α** after a) 0 h, b) 1 h, c) 2 h, d) 3 h, and e) 6 h of air aging.

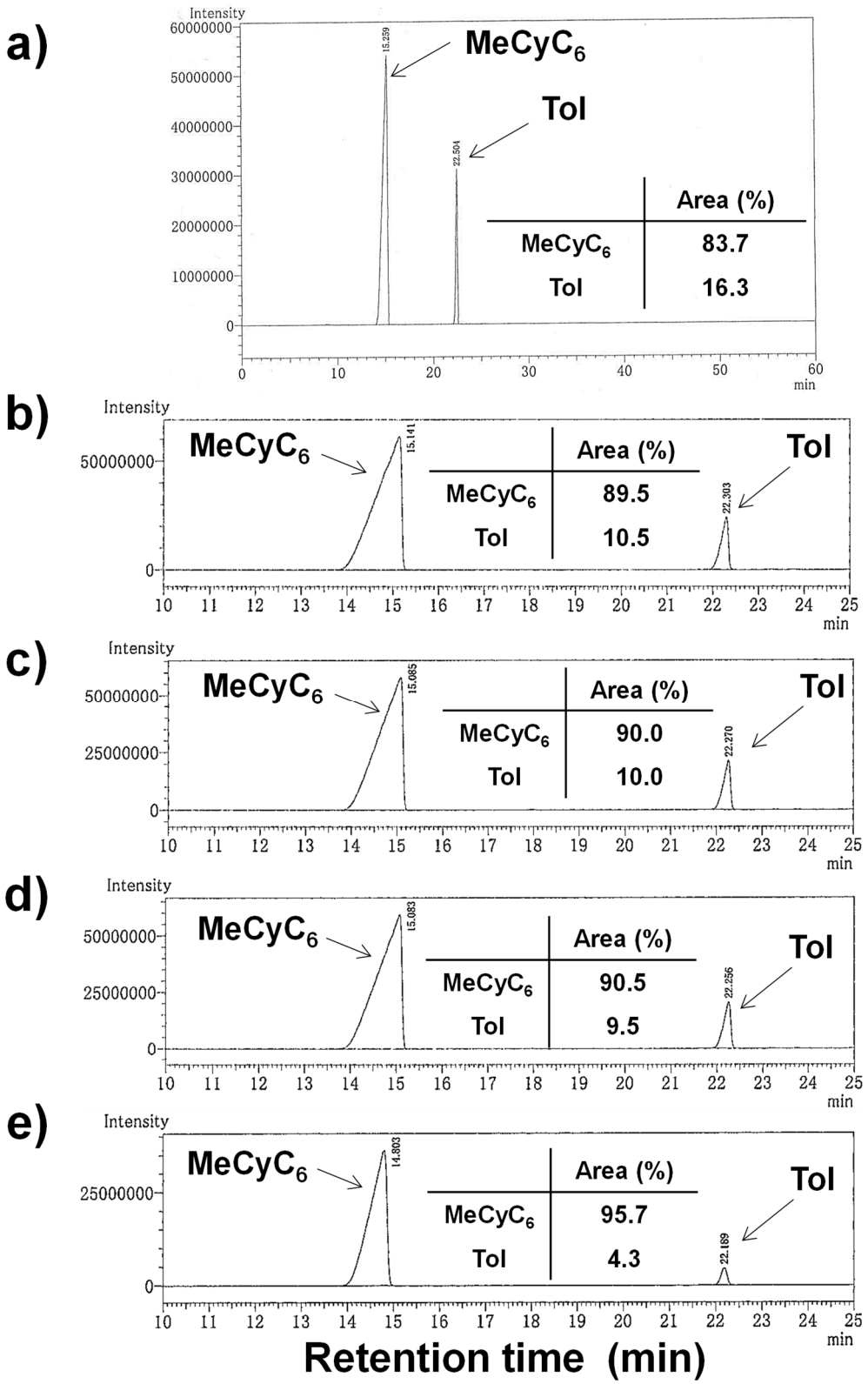

Fig. S8 Preliminary data of head-space gas chromatograms of the remaining ratio of $MeCyC_6$ and Tol in **1α** after a) 0 h, b) 1 h, c) 2 h, d) 3 h, and e) 6 h of air aging.

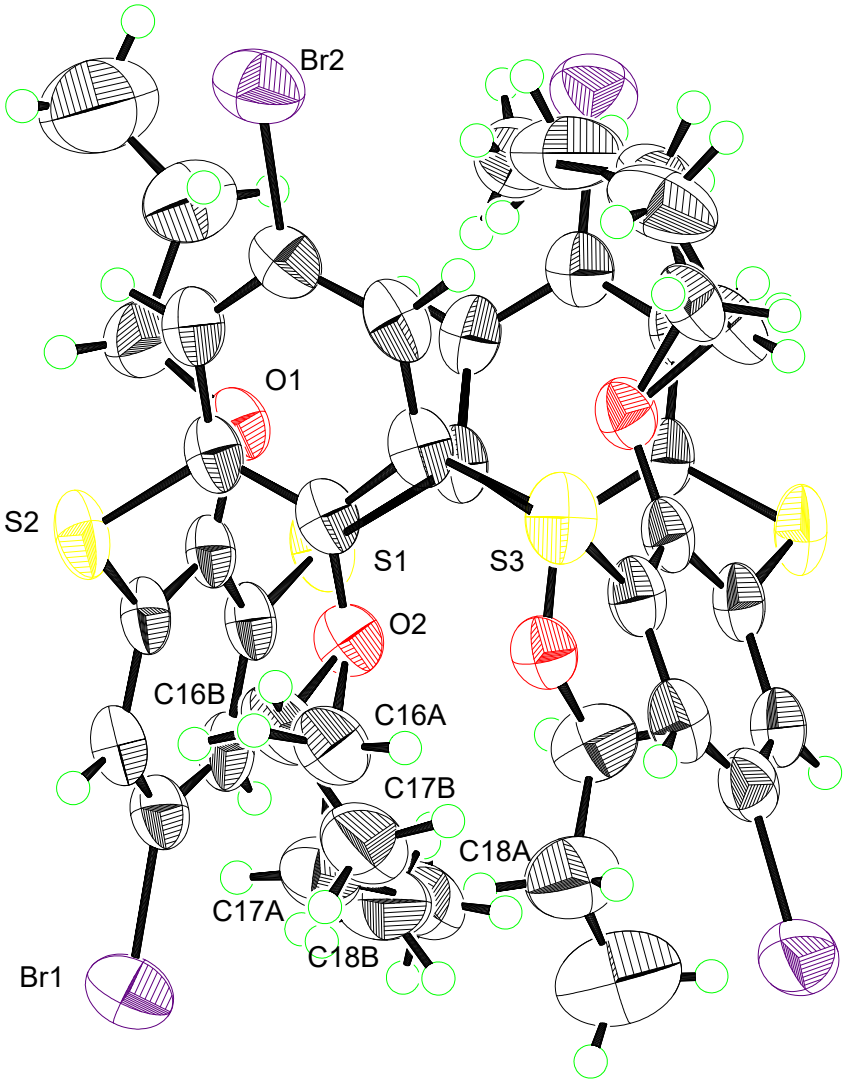

Fig. S9 ORTEP diagram of **1**·MeCyC$_6$ with thermal ellipsoids at 50 % probability. Color code: bromine (purple), sulfur (yellow), oxygen (red), carbon (black), and hydrogen (light green).

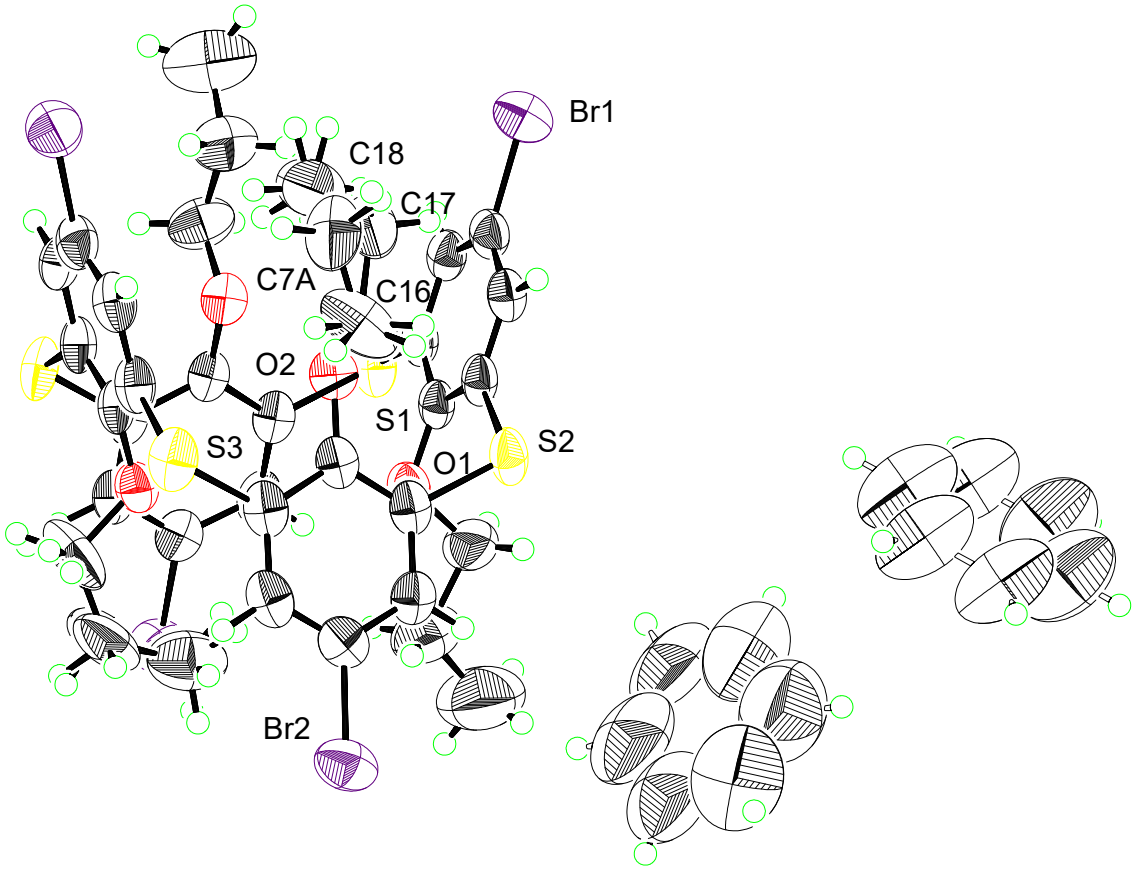

Fig. S10 ORTEP diagram of **1**·Bz with thermal ellipsoids at 50 % probability. Color code: bromine (purple), sulfur (yellow), oxygen (red), carbon (black), and hydrogen (light green).

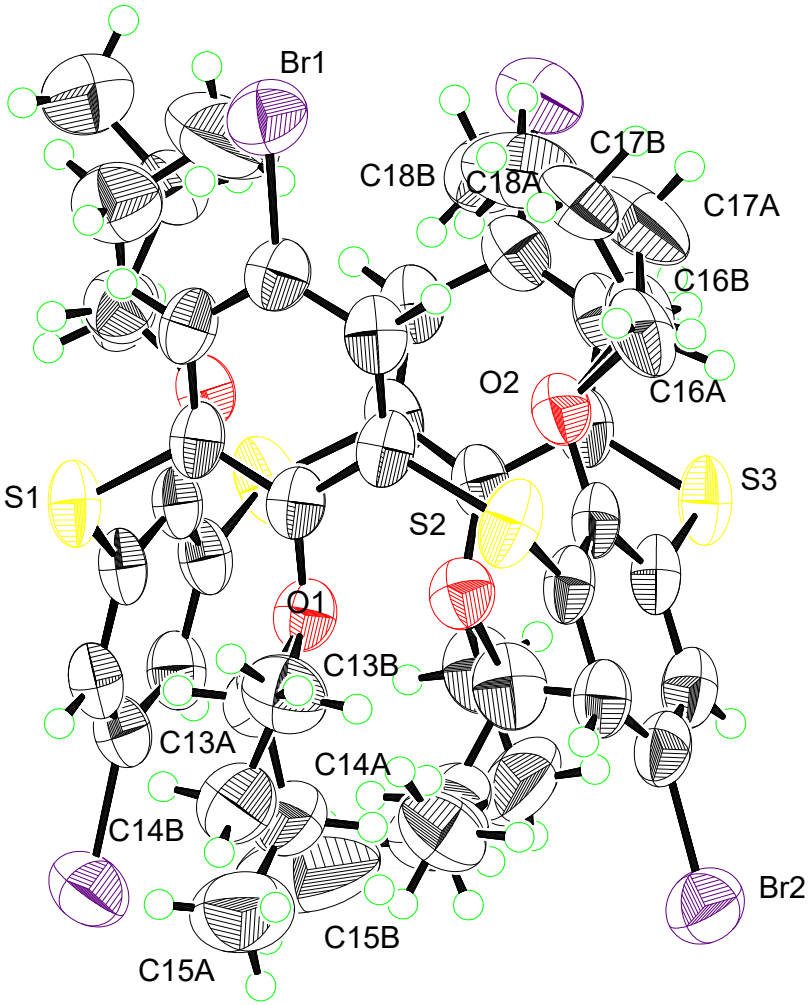

Fig. S11 ORTEP diagram of **1**·Tol with thermal ellipsoids at 50 % probability. Color code: bromine (purple), sulfur (yellow), oxygen (red), carbon (black), and hydrogen (light green).

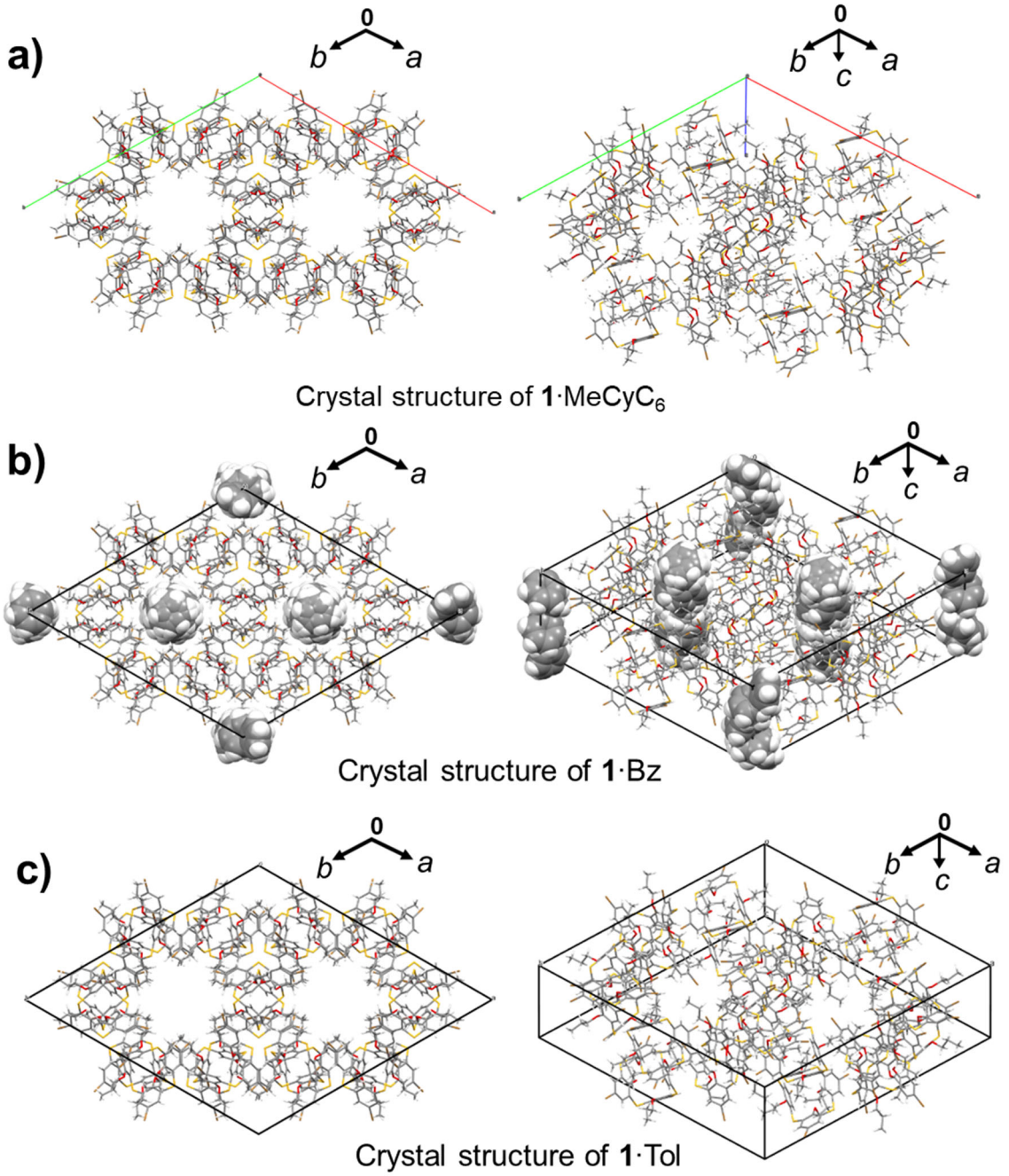

Fig. S12 Extended crystal structures of a) **1**·$MeCyC_6$, b) **1**·Bz, and c) **1**·Tol. These crystal structures were similar to the structure of **1**·CyC_6 (trigonal space group $R\bar{3}c$) reported in our previous work.[S1,S2] Color code: bromine (brown), sulfur (yellow), oxygen (red), carbon (dark gray), and hydrogen (light gray). Bz molecules in the crystal structure of **1**·Bz are shown as space-filling models.

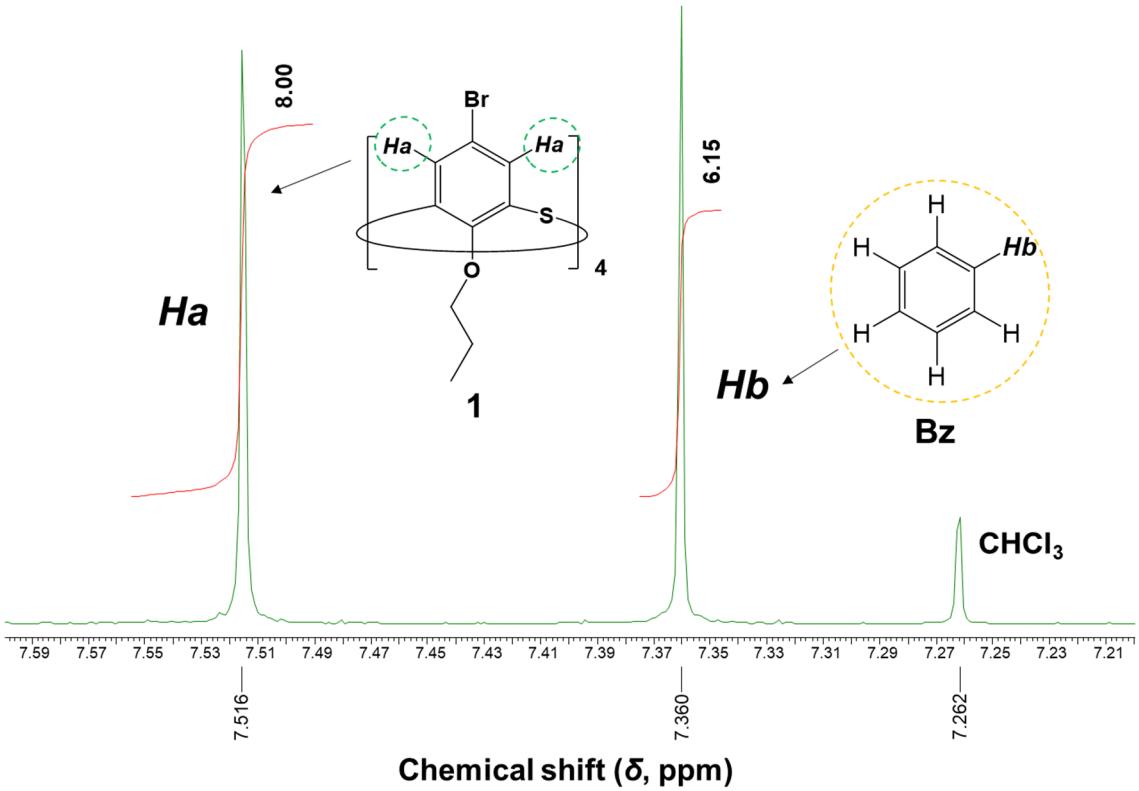

Fig. S13 ^{1}H NMR spectrum of the crystal **1**·Bz dissolved in chloroform-*d*$_1$ ($CDCl_3$, δ from TMS).

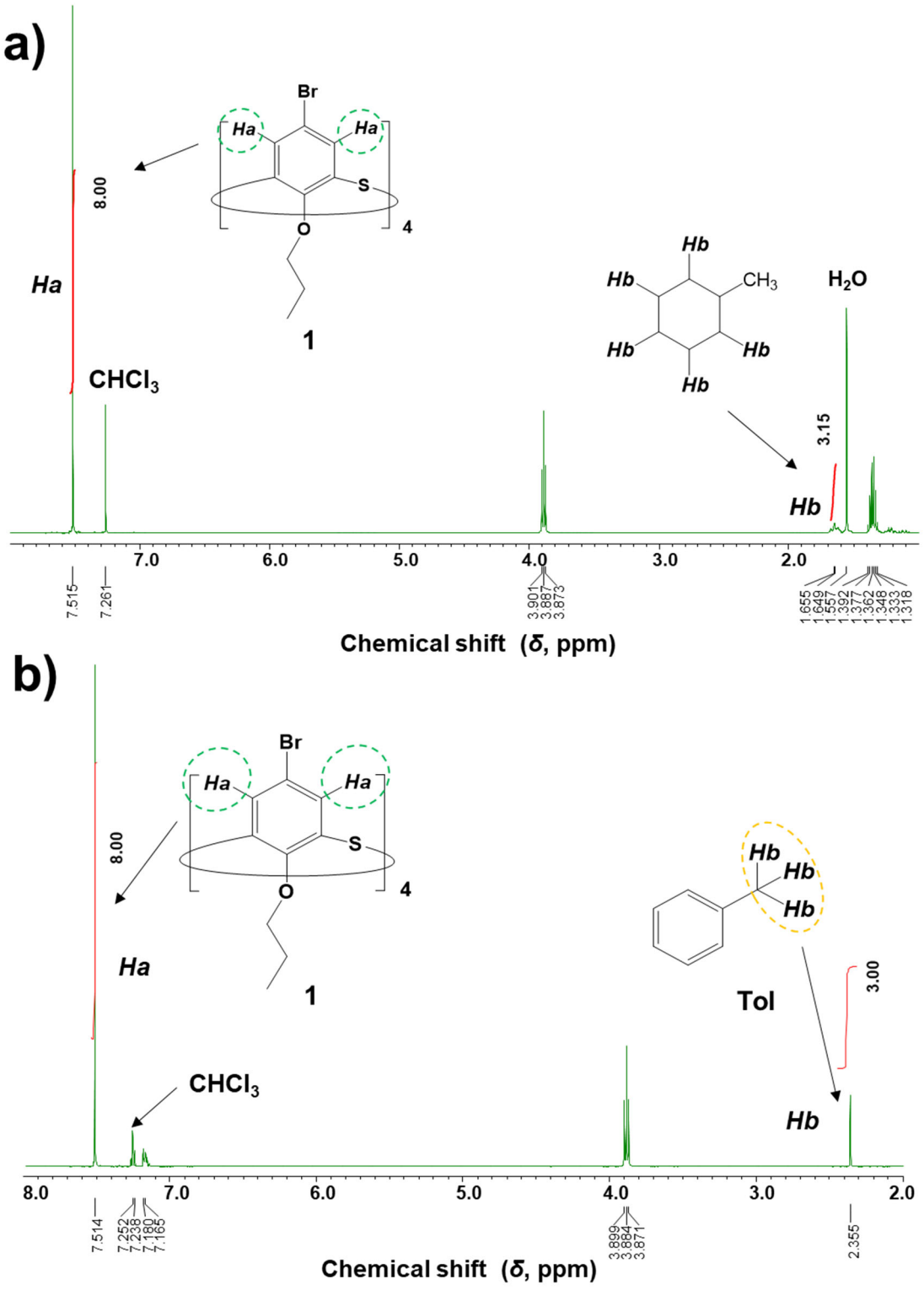

Fig. S14 ^{1}H NMR spectrum of the crystal a) **1**·MeCyC$_6$ and b) **1**·Tol dissolved in chloroform-*d*$_1$ (500 MHz, CDCl$_3$, δ from TMS).

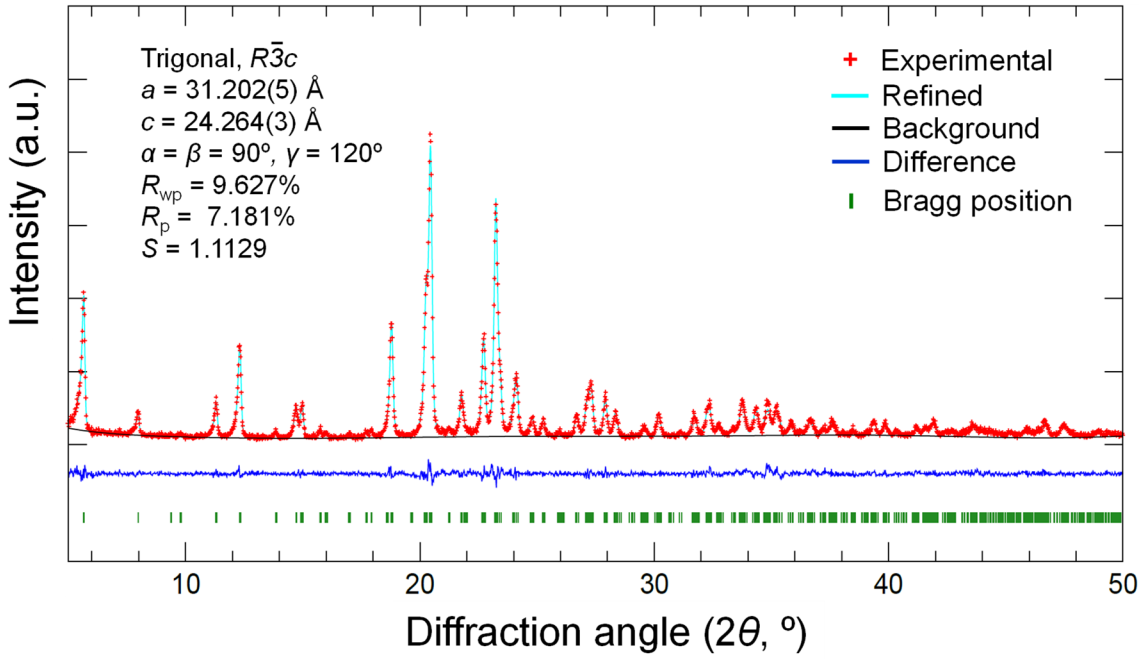

Fig. S15 Le Bail fit for the **1α**-adsorbed $MeCyC_6$ against the experimental powder X-ray diffraction (PXRD) pattern. The red crosses represent the experimental pattern, and the pale blue line represents the refined fit. The background (black), difference plot (blue), and Bragg position (green) are also displayed.

Comparison of the lattice constants of the refined PXRD pattern with those of a single crystal of **1**·$MeCyC_6$:

Lattice constants of the refined PXRD pattern
a = 31.202(5) Å, c = 24.264(3) Å, $\alpha = \beta = 90°$, $\gamma = 120°$

Lattice constants of a single crystal of **1**·$MeCyC_6$
$a = b$ = 31.1921(6) Å, c = 24.1196(5) Å, $\alpha = \beta = 90°$, $\gamma = 120°$

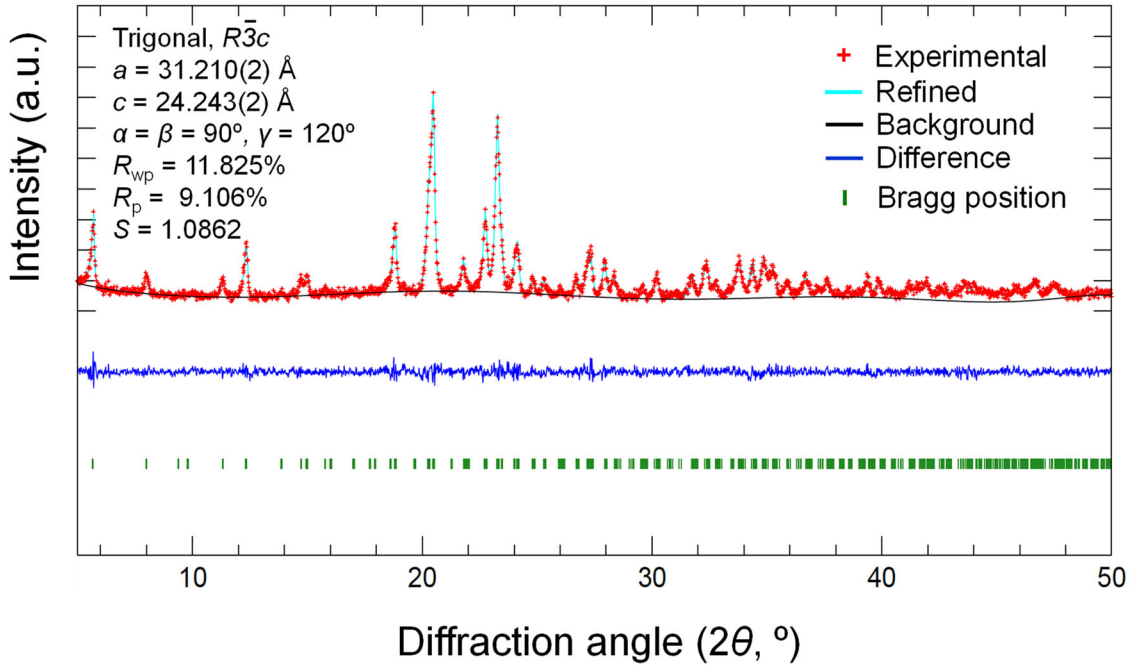

Fig. S16 Le Bail fit for the **1α**-adsorbed Bz against the experimental powder X-ray diffraction (PXRD) pattern. The red crosses represent the experimental pattern, and the pale blue line represents the refined fit. The background (black), difference plot (blue), and Bragg position (green) are also displayed.

Comparison of the lattice constants of the refined PXRD pattern with those of a single crystal of **1**·Bz:

Lattice constants of the refined PXRD pattern
a = 31.210(2) Å, c = 24.232(2) Å, $\alpha = \beta = 90°$, $\gamma = 120°$

Lattice constants of a single crystal of **1**·Bz
$a = b$ = 31.1234(3) Å, c = 24.1605(2) Å, $\alpha = \beta = 90°$, $\gamma = 120°$

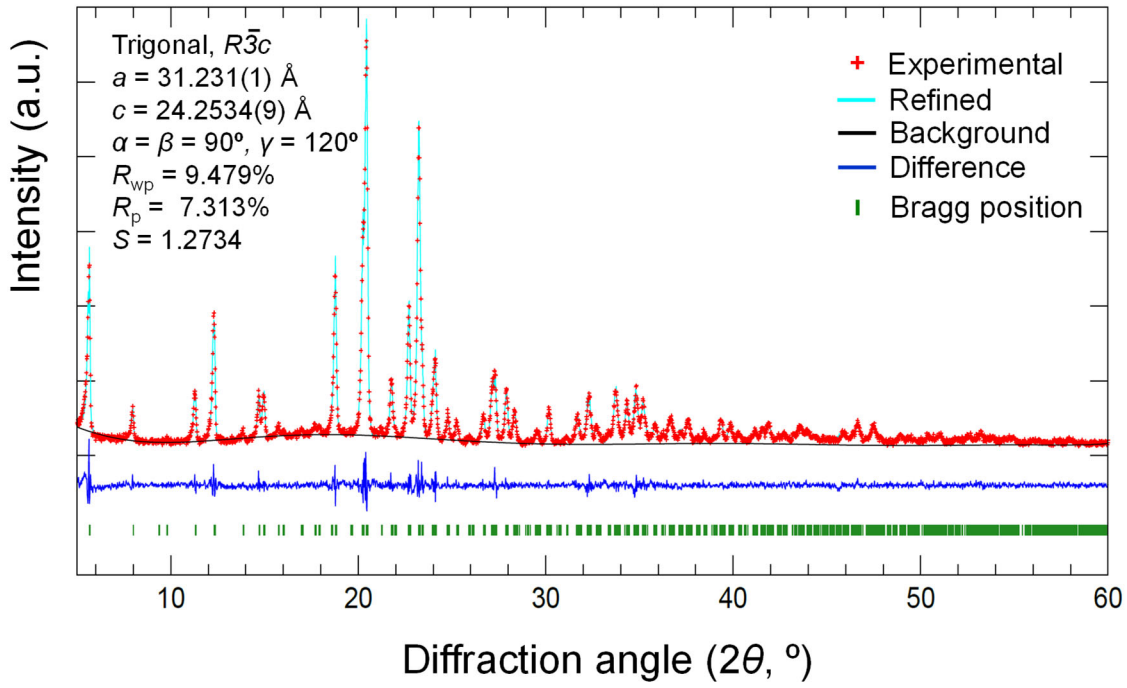

Fig. S17 Le Bail fit for the **1α**-adsorbed Tol against the experimental powder X-ray diffraction (PXRD) pattern. The red crosses represent the experimental pattern, and the pale blue line represents the refined fit. The background (black), difference plot (blue), and Bragg position (green) are also displayed.

Comparison of the lattice constants of the refined PXRD pattern with those of a single crystal of **1**·Tol:

Lattice constants of the refined PXRD pattern
a = 31.286(2) Å, c = 24.228(1) Å, $\alpha = \beta = 90°$, $\gamma = 120°$

Lattice constants of a single crystal of **1**·Tol
$a = b$ = 31.2941(5) Å, c = 24.1681(4) Å, $\alpha = \beta = 90°$, $\gamma = 120°$

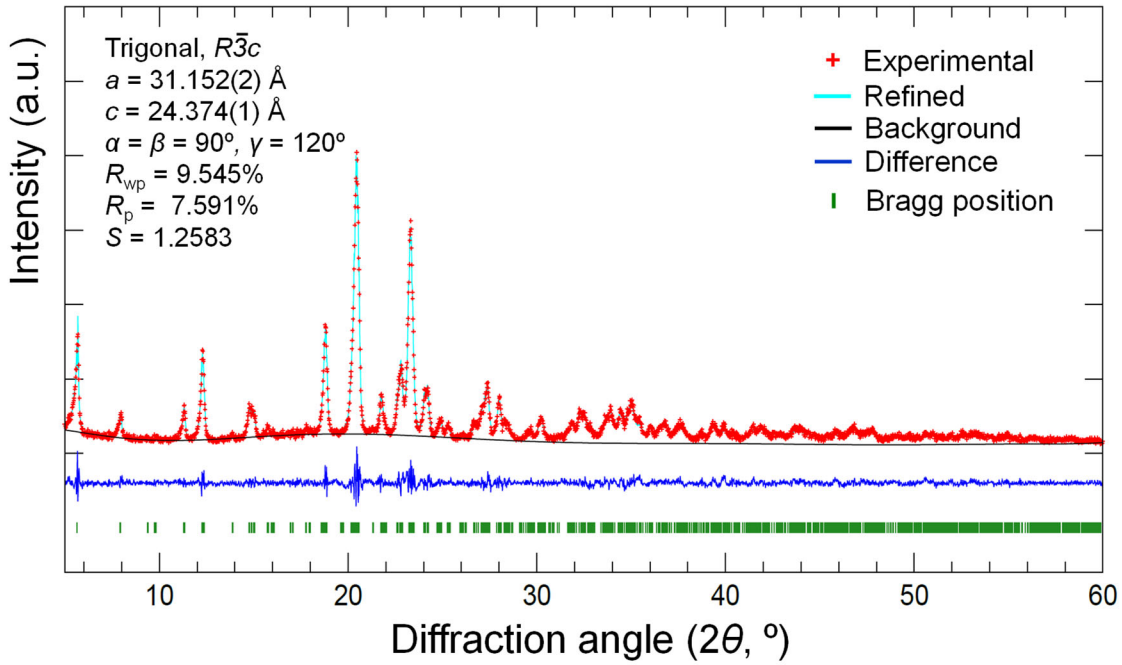

Fig. S18 Le Bail fit for the **1α**-adsorbed CyC_6/Bz against the experimental powder X-ray diffraction (PXRD) pattern. The red crosses represent the experimental pattern, and the pale blue line represents the refined fit. The background (black), difference plot (blue), and Bragg position (green) are also displayed.

Comparison of the lattice constants of the refined PXRD pattern with those of a single crystal of **1**·Bz:

Lattice constants of the refined PXRD pattern
a = 31.152(2) Å, c = 24.374(1) Å, $\alpha = \beta = 90°$, $\gamma = 120°$

Lattice constants of a single crystal of **1**·Bz
$a = b$ = 31.1234(3) Å, c = 24.1605(2) Å, $\alpha = \beta = 90°$, $\gamma = 120°$

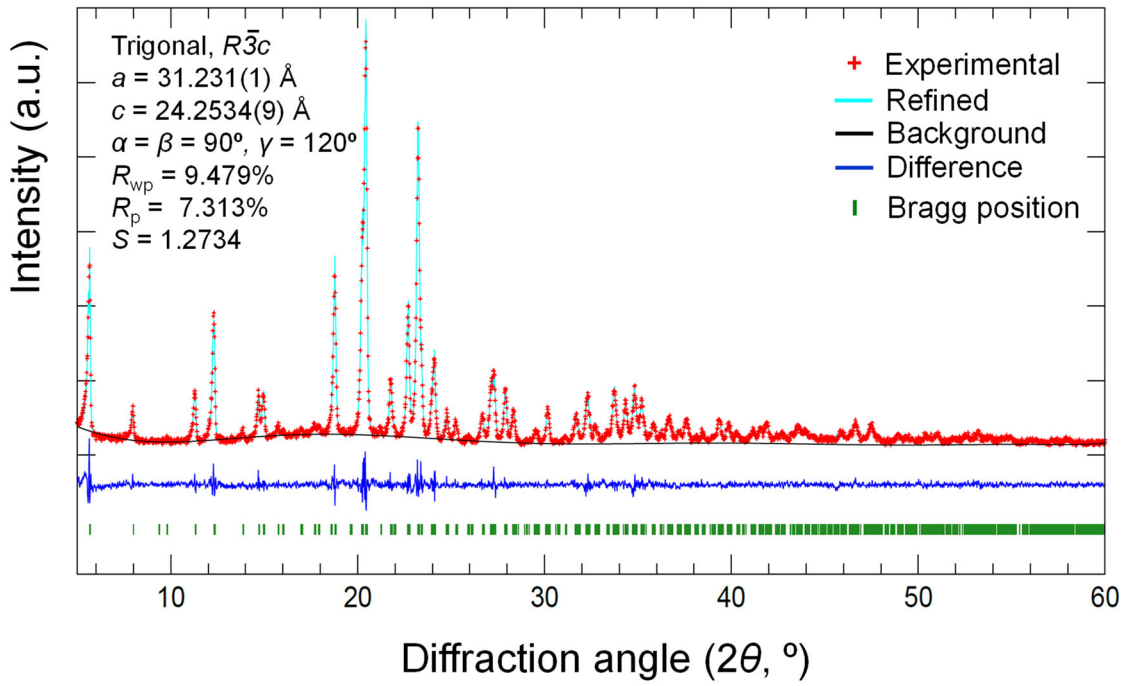

Fig. S19 Le Bail fit for the **1α**-adsorbed MeCyC$_6$/Tol against the experimental powder X-ray diffraction (PXRD) pattern. The red crosses represent the experimental pattern, and the pale blue line represents the refined fit. The background (black), difference plot (blue), and Bragg position (green) are also displayed.

Comparison of the lattice constants of the refined PXRD pattern with those of a single crystal of **1**·Tol:

Lattice constants of the refined PXRD pattern
a = 31.231(1) Å, c = 24.2534(9) Å, $\alpha = \beta = 90°$, $\gamma = 120°$

Lattice constants of a single crystal of **1**·Tol
$a = b$ = 31.2941(5) Å, c = 24.1681(4) Å, $\alpha = \beta = 90°$, $\gamma = 120°$

3. References

S1 F. Hamada, M. Yamada, Y. Kondo, S. Ito and U. Akiba, *CrystEngComm*, **2011**, *13*, 6920-6923.

S2 M. Yamada, F. Uemura, U. M. R. Kunda, T. Tanno, H. Katagiri and F. Hamada, *Chem. Eur. J.* **2020**, *26*, 8393−8399.

S3 G. M. Sheldrick, *Acta Cryst.* **2015**, *A71*, 3–8.

S4 G. M. Sheldrick, *Acta Cryst.* **2015**, *C71*, 3–8

S5 O. V. Dolomanov, L. J. Bourhis, R. J. Gildea, J. A. K. Howard, H. Puschmann, *J. Appl. Cryst.* **2009**, *42*, 339-341

S6 K. Wakita, Yadokari-XG, *Software for Crystal Structure Analyses*, **2001**.

S7 C. Kabuto, S. Akine, T. Nemoto and E. Kwon, *J. Cryst. Soc. Jpn.* **2009**, *51*, 218–224.

S8 A. L. Speck, *Acta Cryst.* **2015**, *C71*, 9–18

S9 A. Le Bail, H. Duroy and J. L. Fourquet, *Mater. Res. Bull.* **1988**, 23, 447–452.

S10 F. Izumi and K. Momma, *Solid State Phenom.*, **2007**, 130, 15–20.